Biomechanical in vitro examination of a standardized low-volume tubular femoroplasty

Horbach, Andreas J ; Staat, Manfred ; Pérez-Viana, Daniel ; Simmen, Hans-Peter ; Neuhaus, Valentin ; Pape, Hans-Christoph ; Prescher, Andreas ; Ciritsis, Bernhard

Abstract: BACKGROUND Osteoporosis is associated with the risk of fractures near the hip. Age and comorbidities increase the perioperative risk. Due to the ageing population, fracture of the proximal femur also proves to be a socio-economic problem. Preventive surgical measures have hardly been used so far. METHODS 10 pairs of human femora from fresh cadavers were divided into control and low-volume femoroplasty groups and subjected to a Hayes fall-loading fracture test. The results of the respective localization and classification of the fracture site, the Singh index determined by computed tomography (CT) examination and the parameters in terms of fracture force, work to fracture and stiffness were evaluated statistically and with the finite element method. In addition, a finite element parametric study with different position angles and variants of the tubular geometry of the femoroplasty was performed. FINDINGS Compared to the control group, the work to fracture could be increased by 33.2%. The fracture force increased by 19.9%. The used technique and instrumentation proved to be standardized and reproducible with an average poly(methyl methacrylate) volume of 10.5 ml. The parametric study showed the best results for the selected angle and geometry. INTERPRETATION The cadaver studies demonstrated the biomechanical efficacy of the low-volume tubular femoroplasty. The numerical calculations confirmed the optimal choice of positioning as well as the inner and outer diameter of the tube in this setting. The standardized minimally invasive technique with the instruments developed for it could be used in further comparative studies to confirm the measured biomechanical results.

DOI: https://doi.org/10.1016/j.clinbiomech.2020.105104

Biomechanical in vitro examination of a standardized low-volume tubular femoroplasty

Andreas J. Horbach[a], Manfred Staat[a,1,*], Daniel Pérez-Viana[a], Hans-Peter Simmen[b], Valentin Neuhaus[b], Hans-Christoph Pape[b], Andreas Prescher[c], Bernhard Ciritsis[d]

[a] *FH Aachen University of Applied Sciences, Institute of Bioengineering, Biomechanics Lab., Heinrich-Mußmann-Straße 1, 52428 Jülich, Germany*
[b] *Universitätsspital Zürich, Trauma Unit, Rämistrasse 100, 8091 Zürich/ Switzerland*
[c] *Institute of Anatomy and Cell Biology, Rheinisch-Westfälische Technische Hochschule Aachen University, Wendlingweg 2, 52074 Aachen/ Germany*
[d] *Ente Ospedaliero Cantonale Ospedale di Bellinzona e Valli, Trauma Unit, Via Ospedale 12, 6500 Bellinzona , Switzerland*

Abstract

Background

Osteoporosis is associated with the risk of fractures near the hip. Age and comorbidities increase the perioperative risk. Due to the ageing population, fracture of the proximal femur also proves to be a socio-economic problem. Preventive surgical measures have hardly been used so far.

Methods

10 pairs of human femora from fresh cadavers were divided into control and low-volume femoroplasty groups and subjected to a Hayes fall-loading fracture test. The results of the respective localization and classification of the fracture site, the Singh index determined by computed tomography (CT) examination and the parameters in terms of fracture force, work to fracture and stiffness were evaluated statistically and with the finite element method. In addition, a finite element parametric study with different position angles and variants of the tubular geometry of the femoroplasty was performed.

Findings

Compared to the control group, the work to fracture could be increased by 33.2%. The fracture force increased by 19.9%. The used technique and

*Corresponding Author

instrumentation proved to be standardized and reproducible with an average poly(methyl methacrylate) volume of 10.5 ml. The parametric study showed the best results for the selected angle and geometry.

Interpretation

The cadaver studies demonstrated the biomechanical efficacy of the low-volume tubular femoroplasty. The numerical calculations confirmed the optimal choice of positioning as well as the inner and outer diameter of the tube in this setting. The standardized minimally invasive technique with the instruments developed for it could be used in further comparative studies to confirm the measured biomechanical results.

Key words: Femoroplasty, Biomechanical Test, Prevention, Proximal Femur Fracture, Osteoporosis

---

Words in Abstract: 249; Words in Text: 3600

1. Introduction

Osteoporosis, which affects over 75 million people, is a widespread disease that primarily affects elderly people (WHO (2003)). In Europe and the USA alone, more than 2.3 million osteoporotic fractures occur every year, with hip fractures being of particular importance from an accident surgery point of view. It is estimated that the number of these fractures will rise to 3 million in 2025 (WHO (2003)). Depending on the report, the 1-year mortality rate is between 14% and 58% (Braithwaite et al. (2003), Mariconda et al. (2015)) with estimated acute health care costs of over USD 86,900 per patient (Frick et al. (2010)). An additional consequence is admission to long-term care facilities. (Cooper (1997)) The risk of further fractures in the proximal femur also increases by a factor of 2.5 (Colón-Emeric et al. (2003)).
Femoroplasty could prove to be a surgical contribution to fracture prevention. It has been defined in the past as augmentation of the medullary canal in the femoral neck using poly(methyl methacrylate) (PMMA) (Beckmann et al. (2011), Heini et al. (2004), Sutter et al. (2010a)). This led to an improvement of the biomechanical properties, which resulted in an increase of the fracture strength in vitro. (Heini et al. (2004)) Furthermore, it has already been shown in vitro that osteosynthesis procedures can be successfully performed on fractures of the proximal femur despite femoroplasty (Beckmann et al. (2007)).

Limiting factors of previous techniques included excessive volumes of the introduced PMMA with the theoretical risk of osteonecrosis by high temperatures during in vivo polymerisation, increased stiffness and uncertainty of the optimal positioning and geometry (Beckmann et al. (2007), Merz et al. (2015), Heini et al. (2004)).

To avoid these problems, low-volume femoroplasty in tubular form was developed using specific surgical instruments (Ciritsis (2017)). Regarding existing work with individualized procedures (Basafa et al. (2013), Basafa and Armand (2014), Basafa et al. (2015)), no standardized procedure to simplify femoroplasty was described in literature right now. With the new developed specific surgical instruments, no individualization of the femoroplasty was required: it is a procedure in which the positioning and insertion of the PMMA are standardized and easily reproducible. Additionally, the monomer of PMMA is known to be cardio toxic (Aebli et al. (2003), Peebles et al. (1972)). To improve flow properties during injection and to reduce toxic side effects in vivo, a high viscosity PMMA and a low injection pressure were used. In order to reduce the amount of PMMA injected and at the same time increase the fracture strength but not the stiffness, a hollow body with defined internal and external dimensions was injected into the bone instead of a solid body.

Other studies (Beckmann et al. (2007), Hofmann-Fliri et al. (2012), Springorum et al. (2014), Sutter et al. (2010b)) show that the geometry and positioning of PMMA in the femoral neck play an important biomechanical role. For this reason, a parametric study for different positioning angles and inner diameters of the tubular PMMA insertion was performed on the basis of existing finite element models to assess the selected geometry and orientation given by the developed surgical tools.

The aim of this work was to test a standardized procedure with focus on geometry, positioning and orientation of the preventive treatment for osteopathic femora with biomechanical experiments and simulations in vitro. Efficiency of the surgical low-volume femoroplasty technique combined with an increase of the fracture force without changing the stiffness were the main criteria to be achieved in this project. It should be clarified which and how certain biomechanical parameters change and to what extent the finite element method can model the experiment for further numerical investigations and variations of femoroplasty.

2. Methods

2.1. Experimental Procedure

10 pairs of human femora were obtained from fresh cadavers of deceased persons who had donated their bodies for research purposes (4 male and 6 female, mean weight 73.4 kg, mean height 171.6 cm, mean age 76.1 years). Between the individual work steps, the cold chain was maintained at -20^{o}C. The temperature of the cadavers was kept at the same level. Before the fracture test, a CT scan and a two-dimensional AP-overview of the femur region with a voltage of 120 kV and a current of 38 mA of each bone pair was taken to determine the Singh index of every femur (Somatom Force, Siemens Healthcare GmbH, Erlangen, Germany). The Singh index, defined in (Singh et al. (1970)), is used as a general indication of osteoporosis in the proximal femur by visually assessing the trabecular pattern as seen on an anteroposterior x-ray image. The grading is based on the disappearance of the five normal trabecular groups and was evaluated independently by two trained physicians. The different grades of the index are shown and explained in Figure1. The Singh index was chosen because it refers directly to the femoral neck and head to be examined. The DEXA scan (dual-energy X-ray absorption measurement) could not be used to determine bone density because the soft tissue envelope of the femora was missing and could not be reliably replaced by a water bath.

Furthermore one of the CTs was used to generate a model for the finite element analysis (FEA) (Figure 3). CT scans revealed no pathological abnormalities other than minor osteoarthritic changes. In order to ensure comparability between the individual bones of the respective pairs, the caput–collum–diaphyseal angle (CCDA) and head diameter in the CT were determined and checked. The body donors were selected so that there were no metastatic pre-existing conditions and they had reached at least 65 years of age.

For the further procedure, the preparations were thawed at room temperature, PMMA (Stryker Simplex HV, aap Biomaterials GmbH, Dieburg, Germany) was introduced in the way described in Ciritsis (2017) using custom-made surgical precision instruments (Safrima AG, Worben, Switzerland) as a standardized tube (inner diameter: 4 mm, outer diameter: 12 mm, length: from the edge of the lateral corticalis of the femoral neck to 10 mm in front of the corticalis at the cortex of the femoral head; "single central") in CCDA-position of the femoral neck and measured the volume used in ml, (Figure 2).

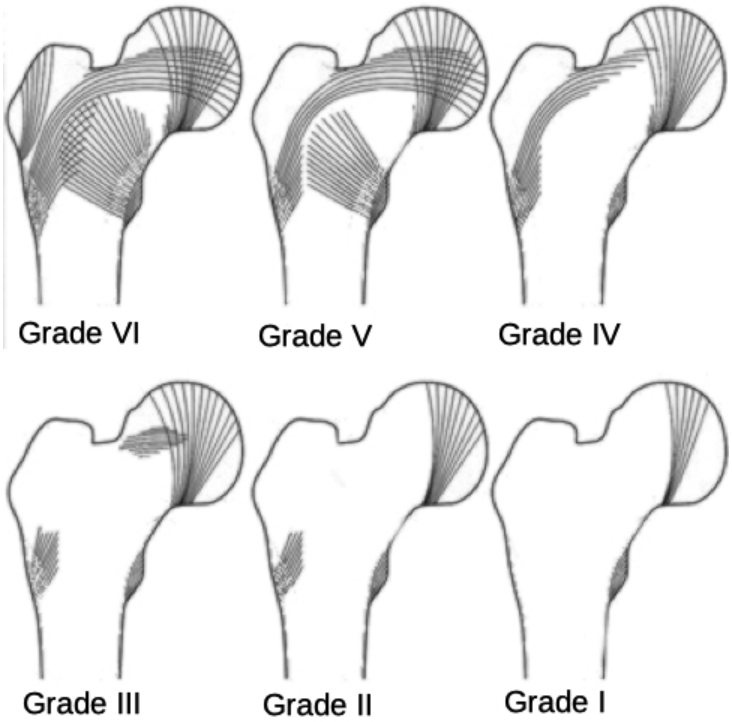

Figure 1: Grades of the Singh index. Grade 6: The five trabecular groups are visible. Grade 5: The principal tensile and principal compressive (medial) group are reduced, and Ward's triangle appears prominent. Grade 4: The principal tensile group is greatly reduced but still connects the lateral cortex to the femoral neck. Grade 3: The principal tensile group is interrupted; this grade indicates definite osteoporosis. Grade 2: The only group present is principal compressive trabeculae. Grade 1: The principal compressive group appears greatly reduced; this grade indicates severe osteoporosis. (Bucholz et al. (2006))

To minimize the influence of biological variance on the statistics, the procedure was tested on ten human bone pairs. Femoroplasty was performed on one bone and the contralateral femur served as a control.

The femora were fixed and loaded analogously to published fracture tests of osteoporotic femora and aligned according to the Hayes fall-loading configuration (Lotz et al. (1995), Lotz and Hayes (1990), Beckmann et al. (2011)). The design is based on the model initially developed by Courtney et al. (1995) and later refined or modified by Lochmüller et al. (2002), Manske et al. (2006), Nishiyama et al. (2013), in which the femur is loaded as in a three-point bending test, Figure 5. To avoid damages of the trochanter

(a) Surgical Tools for PMMA implantation

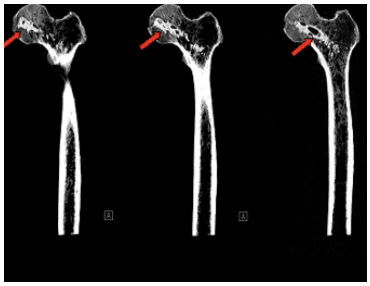

(b) Check of the PMMA tube after implantation via CT-images

(c) Preparation step

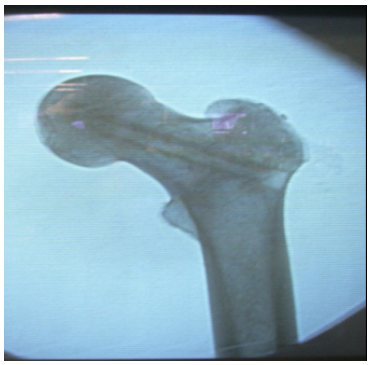

(d) X-Ray image of the femur

Figure 2: Figure 2a: Overview of the developed tools for placement of the PMMA tube in the femoral neck. Figure 2b: Arrows show the holed bone cement tube with small irregularities on its surface, corresponding to the surrounding cancellous bone. Figure 2c: Example of preparation step: The bone cement cylinder was injected and cannulated, the tools are still in place while the bone cement is drying. Figure 2d: PMMA material on the X-ray control after the visible tubular injection.

major and the thin cortical shell of the femur head by direct point loads, the contact area was enlarged by a cushioning half tennis ball as shown in Figure 5c or in Manske et al. (2006).

Each femur was loaded in the test stand by the Z010 material testing machine (Zwick Roell GmbH, Ulm, Germany) with 50 N preload and then with a speed of 10 mm/min until fracture. In addition, the mechanical tests were recorded for optical 3D strain measurement with two digital cameras for digital image correlation (DIC). The femurs were prepared with a speckle pattern which is visible in Figure 5c and is used to analyse the surface motion by

DIC with the software ISTRA4D (Limess Messtechnik und Software GmbH, Krefeld or Dantec Dynamics GmbH, Ulm, Germany) and served to compare the FEA with the experimentally measured deformations in order to confirm the model generated for the FEA.

2.2. Localisation and classification of the fracture area

After each fracture test, the location and type of fracture were determined and photographically documented with a digital camera (NX 2000, Samsung, South Korea) for later evaluation.

2.3. Parameter

Three parameters were determined from the load-displacement curves recorded by the tensile testing machine: work to fracture (Nm), fracture force (N) and stiffness (N/mm) (Figure 4). The fracture force is defined as the first drop of the load-displacement curve after the linear section (point C) at which the macroscopic crack is initiated. This is the point where the bone is defined as fractured, although the crack is not fully through the bone in this test as the little force increase after the drop shows. The work to fracture is the area under the load-displacement curve up to the point of fracture. The elastic property stiffness was calculated as the slope of the load-displacement curve in the linear section of the elastic range (from point A to point B). Above point B, crackling micro cracks were heard and this damage became noticeable in a slight decrease of stiffness. This nonlinear part of the load-displacement curve cannot be compared to the FEA because the evolution of damage has not been simulated. The fracture at point C occurred with a sharply audible crack.

2.4. Statistical Evaluation

To check the normal distribution, the Shapiro-Wilk normality test was performed. Based on its results, the one-sided Wilcoxon signed-rank test was used for paired samples. It was tested whether there was a significant difference in work to fracture, fracture force and stiffness between the two groups. In addition, the Spearman's rank correlation test was performed to check the monotonous correlation between the three main variables and the Singh index. A Spearman's coefficient of $\rho > 0.8$ indicates a strong positive correlation and $\rho > 0.5$ a moderate correlation and the correlation is considered significant if the p-value is $p < 0.05$. All calculations and corresponding diagrams were performed and generated with the R software environment (www.R-Project.org).

2.5. Finite Element Method (FEM)

The femur pair with specimen 3 showed the largest surface with valid DIC measurement. Therefore, the tomogram of this femur pair was selected as representative geometry for FEA. From the obtained CT data a volumetric mesh of the femur was generated with the software Amira v5.5.0 (FEI Visualization Sciences Group, Mérignac Cedex, France). The mesh was segmented to assign a material value to the individual sections depending on their CT intensity for the FEA as given in the table 1 and grouped as shown in Figure 3e and Figure 3f. In supplement to a simple analysis restricted to the bone geometry in Figure 5 and 6, an extended analysis was performed, which included an elastic foundation of the femur head on a cushioning tennis ball.

Different variations of the volume and orientation angle of the tubular PMMA femoroplasty were checked with regard to the stress distribution in the femoral neck by FEM analyses. The Salome v6.6.0 software (Open Cascade SAS, Guyancourt, France) was used as preprocessor and postprocessor and *Code_Aster* vSTA11.4 (Électricité de France, Paris Saclay, France) as FEM solver. A static FEA of the models was performed with the simplifying assumption of isotropic, linear elastic behaviour in all bone regions. Figure 5 shows the boundary conditions with a specific description of the FEM model, which was used analogously to already published studies of femoroplasty and the Hayes fall-loading configuration (Varga et al. (2017), Beckmann et al. (2011)).

Table 1: Overview of the used material parameters for the FEM and the grey scale threshold of the intensity diagrams from Figure 3e and Figure 3f. Region 3 defines the parameters for PMMA (light grey) and the others define the parameters for bone, with region 4 (white area), region 2 (grey area) and region 1 (dark grey area). All regions are shown in Figure 3c and Figure 3d.

Volume region	Young's modulus (MPa)	Poisson Ratio	Inferior Threshold (IU)	Superior Threshold (IU)
Exterior	-	-	min. value	-200
Region 1	300	0.4	-200	200
Region 2	900	0.4	200	800
Region 3 (PMMA)	3300	0.4	800	1350
Region 4 (Corticalis)	15000	0.4	1350	max. value

2.6. Parametric study of the PMMA tube

For an optimized choice of geometries of the PMMA tube, two further possible insertion angles of **CCD**+5° ("single central cranial") and **CCD**−5° ("single central caudal") were selected for the parametric study. In addition, the inner diameter of the tube was varied to the sizes of 2 mm, 4 mm, 6 mm, 8 mm and 10 mm in the calculations. The boundary conditions remained unchanged for all variations. Based on the results of the FEM, the von Mises stresses (MPa) are presented both for the simulation of the experiments and also for the parametric study.

3. Results

Of the ten pairs tested, sixteen femora could be evaluated. Two specimens and thus two pairs were excluded due to failure of the fixation in the fracture test. The average used PMMA volume of all augmented femora was 10.5ml. Table 2 documents an overview of the individual test specimens with corresponding Singh index, fracture type, sex and age. Trochanteric fractures occurred more frequently in the augmented group than in the control group. Fractures in the neck area were less frequent in the augmented group. In one of the prepared femora a subtrochanteric fracture was observed.

3.1. Evaluation of calculated parameters

Table 3, Table 4 and Table 5 provide an overview of the calculated parameters of fracture force, work to fracture and stiffness. The percentage change between control group and augmented femora was determined from the respective mean values. The stiffness and the work to fracture are influenced by the elastic foundation by a half tennis ball and can only be used as relative values to compare the tested femora. A FEM analysis of control sample 1 of the femur showed a calculated stiffness of 1119.3 N/mm, which is almost reduced to the experimental value of 418.4 N/mm when the tennis ball is added to the calculation model. The fracture force, on the other hand, is an absolute value that is not altered by the cushioning bearing.
The statistical evaluation according to the Wilcoxon signed-rank test showed that a significant increase in work to fracture of 33% was achieved by the femoroplasty (14.0 Nm vs. 10.5 Nm, $p = 0.021$). The fracture force also increased significantly by 19.9% in the augmented femora (2998 N vs. 2465 N, $p = 0.054$). The stiffness with a 3.6% increase did not increase significantly (492.8 N/mm vs. 448.6 N/mm, $p = 0.473$). (Figure 6)

Table 2: Complete overview of the evaluated samples.

Sample	Side	Augm.	Sex	Age	Fracture Line	Singh-Index
1	left	yes	male	83	trochant.	I
	right	no			neck	
2	left	yes	male	68	neck	IV
	right	no			neck	
3	left	yes	male	73	trochant.	V
	right	no			neck	
4	left	yes	male	65	trochant.	II
	right	no			trochant.	
5	left	yes	male	66	subtrochant.	III
	right	no			trochant.	
6	left	yes	female	88	trochant.	II
	right	no			trochant.	
7	left	yes	female	83	trochant.	I
	right	no			trochant.	
8	left	yes	female	83	trochant.	II
	right	no			trochant.	

Table 3: Fracture force in (N)

Sample	Augm./ (N)	Control/ (N)	Difference/ (N)	Difference/ %
1	2878	2111.8	766.2	36.3
2	4071.4	4697.2	−625.8	−13.3
3	3324.2	3664.3	−340.1	−9.3
4	2775.9	2387.5	388.4	16.3
5	6571.7	4190.6	2381.1	56.8
6	2861	2346.4	514.6	21.9
7	2147	1210.8	936.2	77.3
8	3117.4	2543	574.4	22.6
mean	3468.3	2894.0	574.4	19.9

3.2. Correlation with the Singh Index

The Spearman's rank correlation showed a significant correlation of the Singh index with fracture force ($\rho_{(8)} = 0.82$, $p = 0.006$) and work to fracture ($\rho_{(8)} = 0.88$, $p = 0.002$) and a moderate correlation with stiffness ($\rho_{(8)} = 0.70$,

Table 4: Work to fracture in (Nm)

Sample	Augm./ (Nm)	Control/ (Nm)	Difference/ (Nm)	Difference/ %
1	15	8.4	6.6	78.6
2	23.3	24.8	−1.5	−6
3	14.1	10.8	3.3	30.6
4	13.5	11.9	1.6	13.4
5	34.2	21.2	13	61.3
6	8.8	10.2	−1.4	−13.7
7	13.9	3.7	10.2	275.7
8	11.2	9.6	1.6	16.7
mean	16.8	12.6	4.2	33.2

Table 5: Stiffness in (N/mm)

Sample	Augm./ (N/mm)	Control/ (N/mm)	Difference/ (N/mm)	Difference/ %
1	469.3	418.4	50.9	12.2
2	443.1	671	−227.9	−34.0
3	516.2	835.6	−319.4	−38.2
4	410.1	314.7	95.4	30.3
5	887.4	590.4	297	50.3
6	573.1	301.9	271.2	89.8
7	157.4	300.2	−142.8	−47.6
8	595.5	478.7	116.8	24.4
mean	506.5	488.9	17.7	3.6

$p = 0.027$) in the control group. The augmented group showed no correlation between the Singh index and work to fracture and stiffness. There was a moderate correlation with the fracture force ($\rho_{(8)} = 0.65$, $p = 0.04$).

3.3. Results of the Finite Element Analysis

The comparison of the experimental strains from the DIC measurements with the measured strains showed that the strain ranges were qualitatively comparable (Figure 7). Differences result from the incomplete knowledge of the elastic material data. The FEA showed a reduction of stress in the medial neck of the augmented femur, which was not found in the control

femur. This is only possible if stress is redistributed so that the load in the augmented femur is transferred through other areas. And indeed, the stresses in the cancellous bone increased significantly near the implant (Figure 8), indicating that the implant contributes to load transfer. This explains the increased carrying capacity of femoroplasty.

The stiffness values of the simplified geometry were 1120 N/mm compared to 469.3 N/mm (extended group) and 418.4 N/mm (control group) from the experiment. The model geometry extended by the tennis ball with rubber material parameters could reach values between 317 N/mm and 598 N/mm.

3.3.1. Results of the parametric study

Figure 9 shows an almost linear increase in the maximum stress with the inner diameter both in the PMMA and in the infero-medial femoral neck region. If the internal diameter is increased by 1 mm, the maximum stress in the femur increases only slightly by 1 MPa, while in PMMA it increases by 3.5 MPa. With larger internal diameters stress in the PMMA increases and fatigue may become a long-term issue (Krause et al. (1988)). There are only small differences between the two insertion angles of $CCDA - 5^o$ and $CCDA + 5^o$.

Results of the FEM of the parametric study are represented exemplarily in Figure 10 for the diameters 4 mm and 10 mm in a sectional view in the sagittal plane. Figures 10a, 10b and 10c show the stress distribution for different positioning angles with a tube diameter of 4 mm. The stresses in the area of the hollow cylinder increase with increasing insertion angle, whereas the stress distribution homogenizes over the entire length of the tube. Figures 10d, 10e and 10f show the range of stress distribution for a tubular PMMA injection with a diameter of 10 mm for the three positioning angles. It is evident that with increasing angle the extension and the magnitude of the maximum stress increases.

4. Discussion

The study is experimentally limited by the number of femora tested and the focus on the experimental setup on the Hayes fall-loading configuration. This could be partly compensated by the parametric study of the FEM. The variation of the geometries also proved that the chosen angulation, inner and outer diameter of the PMMA tubes, which were performed by the used standardized surgical tools, yielded favourable biomechanical results. The

parametric study shows that the reduction of PMMA volume by increasing of the inner diameter is restricted by the fatigue strength of the PMMA but not by the stress in the femur. The biomechanical efficacy of the low-volume tubular femoroplasty could be statistically supported by the data obtained from the test series. Work to fracture and fracture force showed a significant increase of 33% and 19.9%, respectively, compared to the control group. Similar results were obtained in other studies, but with PMMA volumes four to five times larger than in the present study (Heini et al. (2004), van der Steenhoven et al. (2009), van der Steenhoven et al. (2011)) or with individualized femoroplasty (Basafa et al. (2013), Basafa and Armand (2014), Basafa et al. (2015)). A comparison study of high and low volume PMMA using an individualized technique has not yet been published before. A parametric study has therefore been carried out, but it does not yet include any comparisons between the new surgical device technique presented here and already existing techniques.

Remarkably, a nearly unchanged stiffness of the augmented femora was observed, which can be interpreted positively for the physiologically given deformation properties of the femoral neck. Almost unchanged stiffness is a global indicator of reduced stress shielding and bone remodelling by the femoroplasty. The femoral neck is a dominantly cancellous structure with high flexibility. It is known from kyphoplasty that excessive stiffening of the augmented vertebral bodies can lead to secondary fractures of the adjacent osteoporotic segments (Meyer et al. (2019), Leschinger et al. (2018), Ko et al. (2019)). Varga et al. (Varga et al. (2017)) also feared fractures in the adjoining pelvic bone structures, whereby they did not distinguish between force and stiffness. The shape of the tube chosen in this study limited the stiffness under axial load of the femoral shaft while maintaining the stiffness and force under bending load. Thus, the required reinforcement of the femoral shaft was achieved without any relevant increase in stiffness. This could be achieved by the selected geometry with an inner diameter of 4 mm, an outer diameter of 12 mm and the alignment angle in the sense of the CCDA of the PMMA tube, which was confirmed by the FEM parametric analysis in this study (Figure 10). With respect to Figure 10c and Figure 10f, it should be noted that a variation of $\mathbf{CCDA} + 5^\circ$ can be considered as a surgical failure. In this study, the Singh index was the only parameter used to determine the grade of osteoporosis of the proximal femur. In contrast to the control group, the small volume tubular femoroplasty led to independence of the Singh index and the associated grade of osteoporosis of the augmented femoral neck

region.
In addition, the results showed that the developed instruments provided a simple and reproducible technique for formation and positioning a geometrically defined PMMA tubular insertion in the femoral neck. It is also worth mentioning that the standardized PMMA tube ends at the lateral edge of the corticalis of the femoral neck and fills it. This could have prevented a weakening of the corticalis due to cavity formation. The used PMMA volumes with an average of 10.5 ml remained very low compared to the already described values from the literature (Heini et al. (2004), Sutter et al. (2010a)) and make osteonecrosis due to heat generation unlikely. In addition, a highly viscous bone cement was used to prevent the toxic monomer of PMMA from spreading beyond the canal drilled for tubular augmentation.
Our experiments also provide guidance as to when femoroplasty may not be appropriate. Sample 2 showed a deterioration of the values for all investigated parameters of strength and sample 3 showed a deterioration of the values for two parameters (fracture force and stiffness). This may be due to poor anchoring of the implant in the cancellous structure of the bone, which can only transmit a lower stress. It is noteworthy that both samples showed the highest Singh index. This was also shown in the results of the control group for the same samples that were among those with the highest fracture force and stiffness (Table 3 and Table 5). For the fracture force and work to fracture, which determine the bearing capacity, it can be observed that the femora weakened by osteoporosis benefits from a very significant strengthening in all fracture tests, while femora without signs of osteoporosis undergo only a tolerable loss of bearing capacity in individual cases.
In summary, the biomechanical properties of osteoporotic proximal femur could be significantly improved by the low-volume tubular femoroplasty in single central position and in CCDA position. Whether these positive experimental results also lead to a reduction of the fracture risk in vivo as a surgical preventive measure cannot be proven at present.

5. Conclusions

In this study, a small volume tubular femoroplasty was investigated as an alternative to existing experimental surgical methods. The techniques standardized with the used instruments proved to be reproducible and led to a significant improvement of fracture properties in augmented femora in

vitro. The question arises whether the risk of fracture could be reduced by strengthening the trabecular structure with small volume tubular femoroplasty as preventive surgical cement augmentation. Future investigations, such as comparative studies between high and low volume techniques, must show whether the described preventive measures can lead to better clinical results.

Conflict of interest disclosure

The authors are not compensated and there are no other institutional subsidies, corporate affiliations, or funding sources supporting this work unless clearly documented and disclosed.
There were no conflicts of interest.

Acknowledgement:

Some of the FEM analyses were prepared by Alexander Abel and Lars Hirt as part of their bachelor thesis under the direction of Prof. Dr.-Ing. Manfred Staat.

References

Aebli, N., Krebs, J., Schwenke, D., Davis, G., Theis, J.C., 2003. Pressurization of vertebral bodies during vertebroplasty causes cardiovascular complications - an experimental study in sheep. Spine 28, 1513–1519; discussion 1519–1520. doi:10.1097/01.BRS.0000076830.77134.CB.

Basafa, E., Armand, M., 2014. Subject-specific planning of femoroplasty: A combined evolutionary optimization and particle diffusion model approach. Journal of Biomechanics 47, 2237–43. doi:10.1016/j.jbiomech.2014.05.002.

Basafa, E., Armiger, R.S., Kutzer, M.D., Belkoff, S.M., Mears, S.C., Armand, M., 2013. Patient-specific finite element modeling for femoral bone augmentation. Med Eng Phys 35, 860–865. doi:10.1016/j.medengphy.2013.01.003.

Basafa, E., Murphy, R.J., Otake, Y., Kutzer, M.D., Belkoff, S.M., Mears, S.C., Armand, M., 2015. Subject-specific planning of femoroplasty: An

experimental verification study. Journal of Biomechanics 48, 59–64. doi:https://doi.org/10.1016/j.jbiomech.2014.11.002.

Beckmann, J., Ferguson, S.J., Gebauer, M., Luering, C., Gasser, B., Heini, P., 2007. Femoroplasty - augmentation of the proximal femur with a composite bone cement – feasibility, biomechanical properties and osteosynthesis potential. Medical Engineering & Physics 29, 755–764. doi:10.1016/j.medengphy.2006.08.006.

Beckmann, J., Springorum, R., Vettorazzi, E., Bachmeier, S., Lüring, C., Tingart, M., Püschel, K., Stark, O., Grifka, J., Gehrke, T., Amling, M., Gebauer, M., 2011. Fracture prevention by femoroplasty-cement augmentation of the proximal femur. Journal of Orthopaedic Research 29, 1753–8. doi:10.1002/jor.21410.

Braithwaite, R.S., Col, N.F., Wong, J.B., 2003. Estimating hip fracture morbidity, mortality and costs. Journal of the American Geriatrics Society 51, 364–370. doi:10.1046/j.1532-5415.2003.51110.x.

Bucholz, R.W., Court-Brown, C.M., Heckman, J.D., Tornetta III, P., 2006. Rockwood and Green's Fractures in Adults. 92. 7th edition ed., Lippincott Williams & Wilkins, Philadelphia.

Ciritsis, B., 2017. Surgical Tool System. Patent EP2806807B1. Unitectra Zürich. patents.google.com/patent/EP2806807A1/en.

Colón-Emeric, C., Kuchibhatla, M., Pieper, C., Hawkes, W., Fredman, L., Magaziner, J., Zimmerman, S., Lyles, K.W., 2003. The contribution of hip fracture to risk of subsequent fracture: Data from two longitudinal studies. Osteoporosis International 14, 879–88,. doi:10.1007/s00198-003-1460-x.

Cooper, C., 1997. The crippling consequences of fractures and their impact on quality of life. The American Journal of Medicine 103, S12–S19. doi:10.1016/S0002-9343(97)90022-X.

Courtney, A.C., Wachtel, E.F., Myers, E.R., Hayes, W.C., 1995. Age-related reductions in the strength of the femur tested in a fall-loading configuration. The Journal of Bone and Joint Surgery. American Volume 77, 387–95. doi:10.2106/00004623-199503000-00008.

Frick, K.D., Kung, J.Y., Parrish, J.M., Narrett, M.J., 2010. Evaluating the cost-effectiveness of fall prevention programs that reduce fall-related hip fractures in older adults. Journal of the American Geriatrics Society 58, 136–141. doi:10.1111/j.1532-5415.2009.02575.x.

Heini, P., Franz, T., Fankhauser, C., Gasser, B., Ganz, R., 2004. Femoroplasty-augmentation of mechanical properties in the osteoporotic proximal femur: A biomechanical investigation of PMMA reinforcement in cadaver bones. Clinical Biomechanics (Bristol, Avon) 19, 506–12. doi:10.1016/j.clinbiomech.2004.01.014.

Hofmann-Fliri, L., Sermon, A., Wähnert, D., Schmoelz, W., Blauth, M., Windolf, M., 2012. Limited v-shaped cement augmentation of the proximal femur to prevent secondary hip fractures. Journal of Biomaterials Applications 28. doi:10.1177/0885328212443274.

Ko, B.S., Cho, K.J., Park, J.W., 2019. Early adjacent vertebral fractures after balloon kyphoplasty for osteoporotic vertebral compression fractures. Asian Spine Journal 13, 210–215. doi:10.31616/asj.2018.0224.

Krause, W., Mathis, R.S., Grimes, L.W., 1988. Fatigue properties of acrylic bone cement:S-N,P-N, andP-S-N data. Journal of Biomedical Materials Research 22, 221–244. doi:10.1002/jbm.820221404.

Leschinger, T., Engel, K., Brüggemann, G.P., Dederer, V., Friedrich Neiss, W., Scheyerer, M., Peter Müller, L., Wegmann, K., 2018. Glass-polyalkenoate cement: An alternative material for kyphoplasty in osteoporotic vertebral compression fractures - an ex vivo study. Journal of the Mechanical Behavior of Biomedical Materials 83. doi:10.1016/j.jmbbm.2018.03.008.

Lochmüller, E.M., Groll, O., Kuhn, V., Eckstein, F., 2002. Mechanical strength of the proximal femur as predicted from geometric and densitometric bone properties at the lower limb versus the distal radius. Bone 30, 207–16. doi:10.1016/s8756-3282(01)00621-4.

Lotz, J., Hayes, W., 1990. The use of quantitative computed tomography to estimate risk of fracture of the hip from falls. Journal of Bone and Joint Surgery 72, 689–700. doi:10.2106/00004623-199072050-00008.

Lotz, J.C., Cheal, E.J., Hayes, W.C., 1995. Stress distributions within the proximal femur during gait and falls: implications for osteoporotic fracture. Osteoporosis International 5, 252–261. doi:10.1007/bf01774015.

Manske, S.L., Liu-Ambrose, T., de Bakker, P.M., Liu, D., Kontulainen, S., Guy, P., Oxland, T.R., McKay, H.A., 2006. Femoral neck cortical geometry measured with magnetic resonance imaging is associated with proximal femur strength. Osteoporosis International 17, 1539–45. doi:10.1007/s00198-006-0162-6.

Mariconda, M., Costa, G.G., Cerbasi, S., Recano, P., Aitanti, E., Gambacorta, M., Misasi, M., 2015. The determinants of mortality and morbidity during the year following fracture of the hip. Bone & Joint Journal 97-B, 383–390. doi:10.1302/0301-620X.97B3.34504.

Merz, M.K., Christoforetti, J.J., Domb, B.G., 2015. Femoral neck fracture after arthroscopic femoroplasty of the hip. Orthopedics 38, e696–700. doi:10.3928/01477447-20150804-57.

Meyer, C., Gaalen, K., Leschinger, T., Scheyerer, M., Neiss, W., Staat, M., Mueller, L., Wegmann, K., 2019. Kyphoplasty of osteoporotic fractured vertebrae: A finite element analysis about two types of cement. BioMed Research International 2019, 1–7. doi:10.1155/2019/9232813.

Nishiyama, K.K., Gilchrist, S., Guy, P., Cripton, P., Boyd, S.K., 2013. Proximal femur bone strength estimated by a computationally fast finite element analysis in a sideways fall configuration. Journal of Biomechanics 46, 1231–6. doi:10.1016/j.jbiomech.2013.02.025.

Peebles, D.J., Ellis, R.H., Stride, S.D., Simpson, B.R., 1972. Cardiovascular effects of methylmethacrylate cement. British Medical Journal 1, 349–351. doi:10.1136/bmj.1.5796.349.

Singh, M., Nagrath, A.R., Maini, P.S., 1970. Changes in trabecular pattern of the upper end of the femur as an index of osteoporosis. The Journal of Bone & Joint Surgery 52, 457–467.

Springorum, H.R., Gebauer, M., Mehrl, A., Stark, O., Craiovan, B., Püschel, K., Amling, M., Grifka, J., Beckmann, J., 2014. Fracture prevention by prophylactic femoroplasty of the proximal femur–metallic compared with

cemented augmentation. Journal of Orthopaedic Trauma 28, 403–409. doi:10.1097/bot.0000000000000035.

van der Steenhoven, T., Schaasberg, W., de Vries, A., Valstar, E., Nelissen, R., 2009. Augmentation with silicone stabilizes proximal femur fractures: An in vitro biomechanical study. Clinical Biomechanics 24, 286–290. doi:doi.org/10.1016/j.clinbiomech.2008.11.009.

van der Steenhoven, T., Schaasberg, W., de Vries, A., Valstar, E., Nelissen, R., 2011. Elastomer femoroplasty prevents hip fracture displacement: In vitro biomechanical study comparing two minimal invasive femoroplasty techniques. Clinical Biomechanics 26, 464–469. doi:https://doi.org/10.1016/j.clinbiomech.2010.12.009.

Sutter, E.G., Mears, S.C., Belkoff, S.M., 2010a. A biomechanical evaluation of femoroplasty under simulated fall conditions. Journal of Orthopaedic Trauma 24, 95–99. doi:10.1097/bot.0b013e3181b5c0c6.

Sutter, E.G., Wall, S.J., Mears, S.C., Belkoff, S.M., 2010b. The effect of cement placement on augmentation of the osteoporotic proximal femur. Geriatric Orthopaedic Surgery & Rehabilitation 1, 22–26. doi:10.1177/2151458510378406.

Varga, P., Inzana, J., Schwiedrzik, J., Zysset, P., Gueorguiev, B., Blauth, M., Windolf, M., 2017. New approaches for cement-based prophylactic augmentation of the osteoporotic proximal femur provide enhanced reinforcement as predicted by non-linear finite element simulations. Clinical Biomechanics 44, 7–13. doi:10.1016/j.clinbiomech.2017.03.001.

WHO, 2003. Diet, nutrition and the prevention of chronic diseases, Geneva. Technical Report 916. WHO.

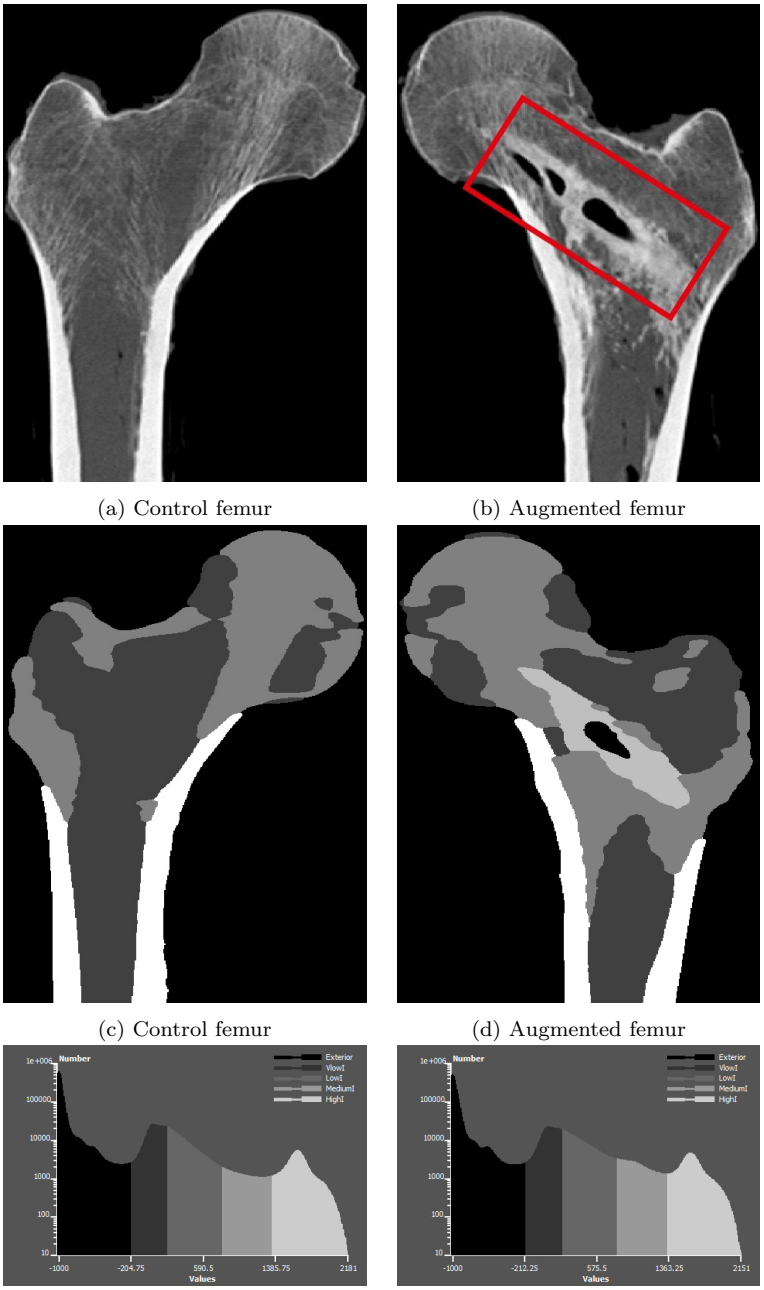

(a) Control femur (b) Augmented femur

(c) Control femur (d) Augmented femur

(e) Control femur (f) Augmented femur

Figure 3: Anterior view of coronal radiographic slices (3a and 3b) and corresponding segmentation label (3c and 3d) of the selected pair of femurs. The cement implant is visible in the augmented femora (right). 3e and 3f show an intensity histograms of the image volumes of the selected pair of femora.

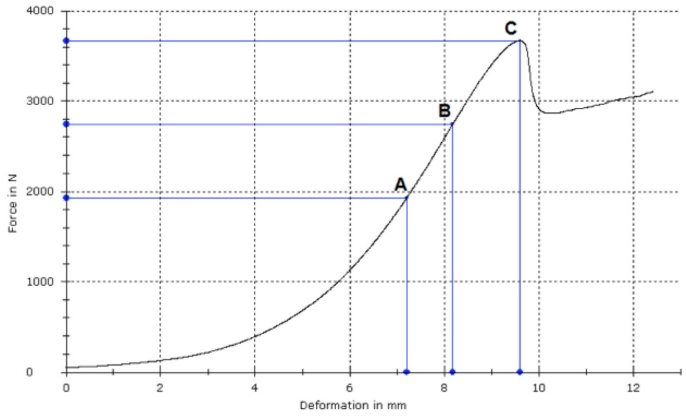

Figure 4: Example illustration of a load-displacement curve with the characteristic points A, B and C. The illustration represents the experimental results for specimen 3-control group.

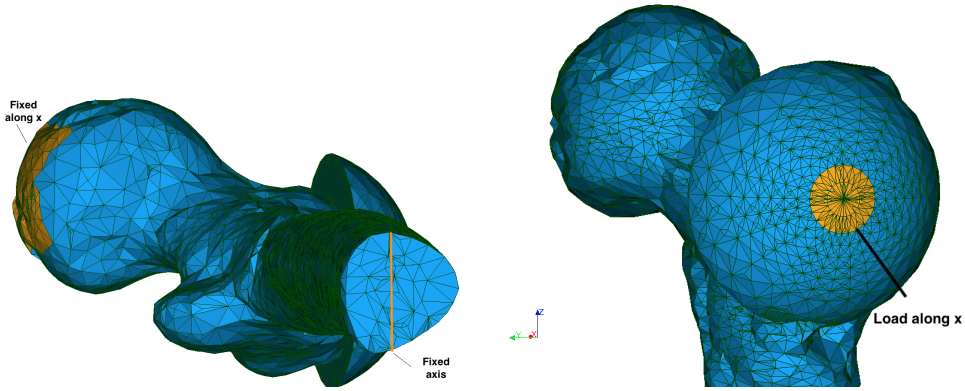

(a) Kinematic boundary conditions (supports)

(b) Static boundary conditions (loading)

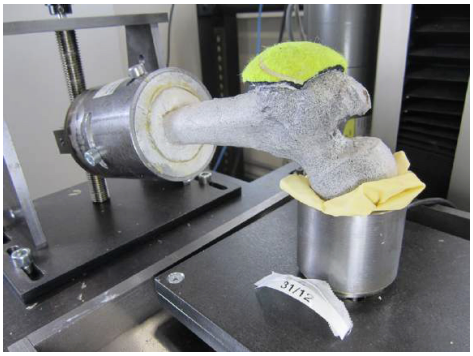

(c) Experimental setup

Figure 5: Figure 5a: Kinematic boundary conditions for the FEA: 1. Cortex of the femur head fixed in x-direction. 2. The cross-section in the proximal third of the femoral diaphysis is fixed such that it can only rotate rigidly about a fixed axis. Figure 5b: The loading in x-direction acts on the trochanter major massif and is distributed by cushioning. Figure 5c: Biomechanical testing device with a human femur fixed for a three-point bending test with cushioning tennis balls. The speckle pattern on the femur is visible.

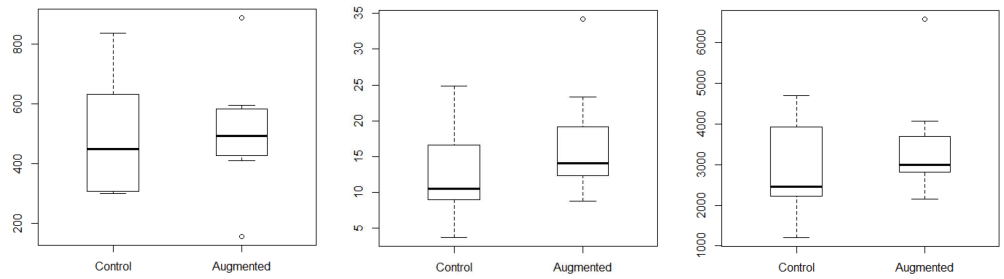

(a) Stiffness (b) Work to fracture (c) Fracture force

Figure 6: Box-and-whisker diagram of (a) stiffness, (b) work to fracture, and (c) fracture force; separated into control group and n augmented femora.

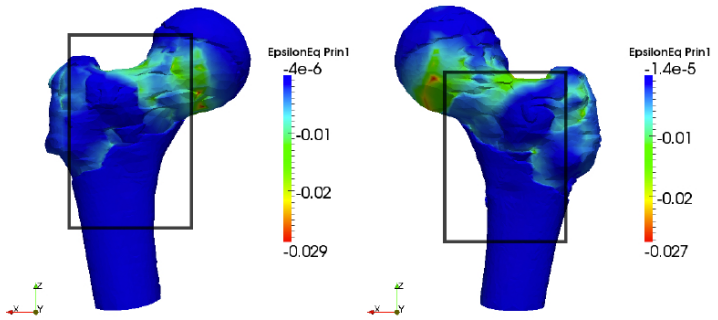

(a) Numerical results of the FEA

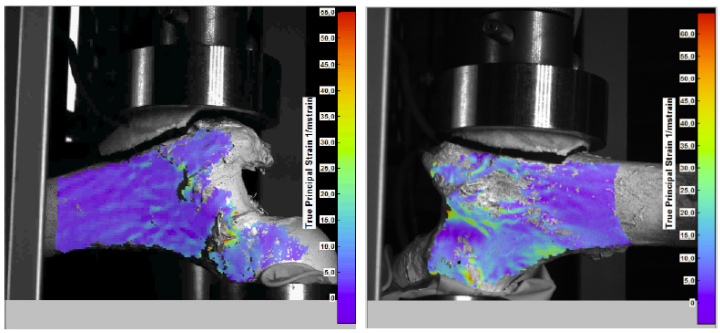

(b) Experimental results of the DIC

Figure 7: Comparison of the major principal strain results of the simulation (7a) and the same results recorded by the ODS (in μstrain) at the moment prior to fracture (7b). The model of the control is on the left and the one of the femoroplasty augmented model is on the right.

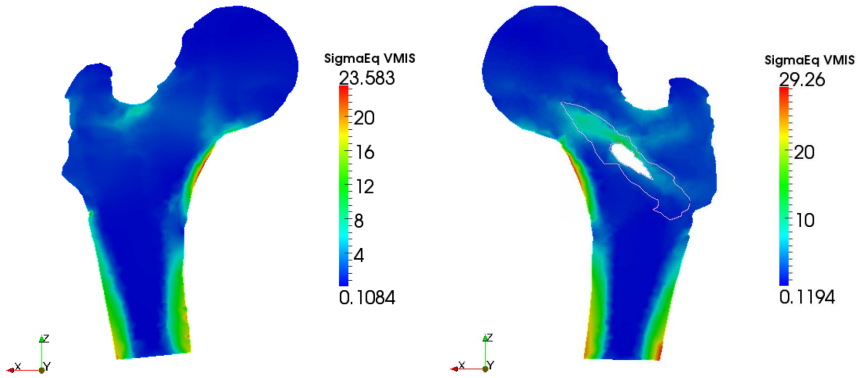

(a) Control bone (b) Augmented bone

Figure 8: Comparison of the von Mises stresses (MPa) in the sagittal plane of the bone from FEA; left control femur and right augmented femur (sample 3), the marked area shows the PMMA tube.

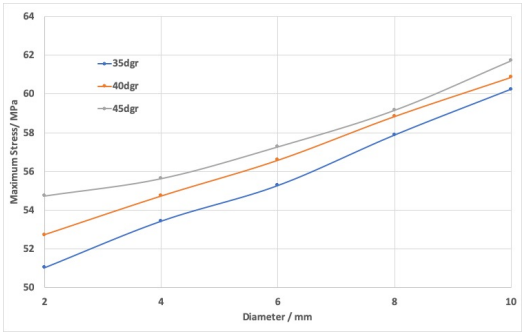

(a) In the femur

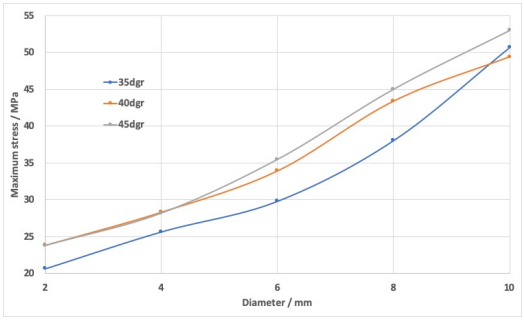

(b) In the tubular PMMA femoroplasty

Figure 9: Maximum value of von Mises stress concentration found in parametric study

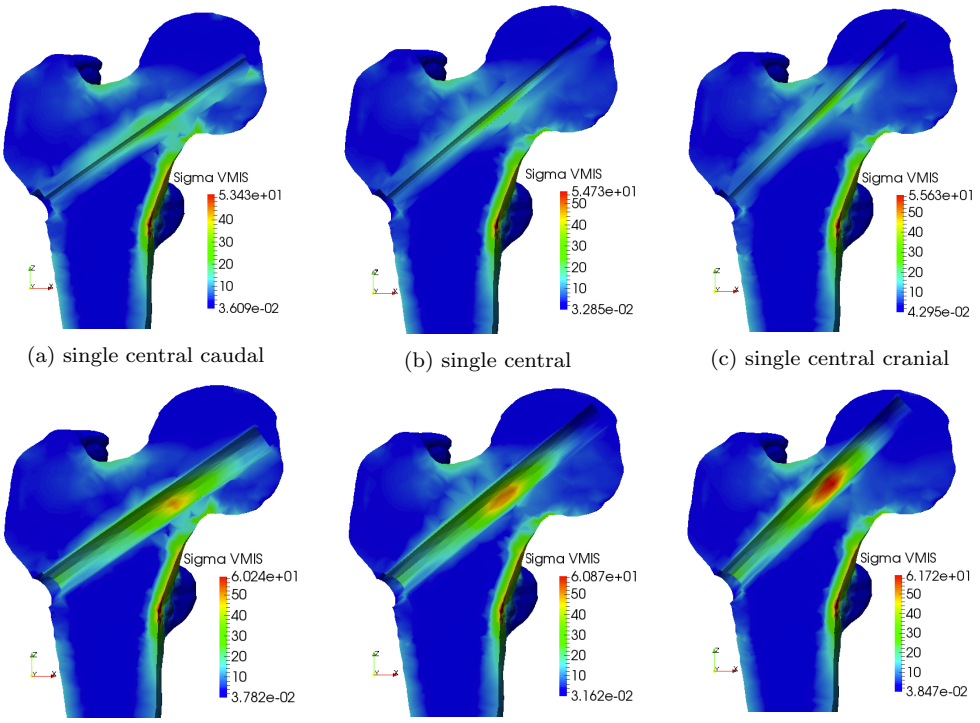

(a) single central caudal (b) single central (c) single central cranial

(d) single central caudal (e) single central (f) single central cranial

Figure 10: Von Mises stresses as results of the parametric study. Figures 10a, 10b and 10c show the stress distribution for an inner diameter of 4 mm and Figures 10d, 10e and 10f for an inner diameter of 10 mm, respectively. All tubes had an outer diameter of 12 mm. Figures 10a and 10d show the results for the angle $\mathbf{CCDA} - 5°$, Figures 10b and 10e for the angle $CCDA$, and Figures 10c and 10f for the angle $\mathbf{CCDA} + 5°$.